

# Effect of ball milling on the phase constitution and microstructure of induction melted Higher Manganese Silicides and their thermoelectric properties

A.J. Zhou<sup>1,2</sup>, X.B. Zhao<sup>1</sup>, T.J. Zhu<sup>1</sup>, E. Mueller<sup>2</sup>, C. Stiewe<sup>2</sup>, R. Hassdorf<sup>2</sup>

1- State Key Laboratory of Silicon Materials, Department of Materials Science and Engineering, Zhejiang University, Hangzhou, 310027, China

2- Institute of Materials Research, German Aerospace Center (DLR), 51147 Köln, Germany

**Abstract:** Pellets of Higher Manganese Silicides (HMS) with a nominal composition of  $Mn_{15}Si_{26}$  were fabricated by inductive levitation melting, followed by ball milling of different duration and hot pressing. The phase constitution and microstructure of the ball-milled powders and the hot-pressed pellets were investigated, and the Seebeck coefficient, the electrical and the thermal conductivity were measured from room temperature to 700 °C. It was found the ball milling process has introduced a phase transformation from HMS to  $MnSi$  (or  $Mn_{1-x}Fe_xSi$ ), and the amount of  $Mn_{1-x}Fe_xSi$  increases with increasing ball milling energy and the milling duration. The average grain size was obviously decreased and reaches nano-scales after ball milling for more than 40 hours. The increasing amount of the  $Mn_{1-x}Fe_xSi$  phase has decreased the Seebeck coefficient, while increased the electrical and the thermal conductivity of the hot-pressed samples, thus deteriorated the thermoelectric performance of the material. The reasons for the phase transformation were discussed in this work with respect to the crystal structure of HMS and its stability under high-energy mechanical impact.

## 1. Introduction

Higher manganese silicides (HMS) are intermetallic compounds with compositions of  $MnSi_x$  ( $x = 1.71-1.75$ ). Much attention has been paid on the study of HMS because of their prospects for optoelectronic and thermoelectric (TE) applications<sup>[1-3]</sup>. In addition to a promising thermoelectric performance ( $ZT_{max} \sim 0.7$ ), their features such as non-toxicity, cheap starting materials, good capacity to be operated in air and in vacuum without any protection and high mechanical strength can fully meet the crucial requirements for the widespread use of TE devices<sup>[4]</sup>. Compared with the state-of-the-art TE materials such as Bi-Te, Pb-Te and Co-Sb based alloys, HMS are of superior positions given their abovementioned characters.

To date studies on TE properties of HMS have been mainly focused on the melt-grown single crystals reported earlier<sup>[5-7]</sup> and recently on HMS thin films<sup>[8-10]</sup>. Reports on polycrystalline HMS are limited. The difficulty that has prevented the systematic study on polycrystalline HMS rests with the special inherent characters of HMS in their varying compositions and phase structures, hence making it difficult to obtain a single phase of HMS via conventional melting processes. Several incommensurate phases, such as  $Mn_4Si_7$ <sup>[11]</sup>,  $Mn_{11}Si_{19}$ <sup>[12]</sup>,  $Mn_{15}Si_{26}$ <sup>[13]</sup> and  $Mn_{27}Si_{47}$ <sup>[14]</sup> have been reported, all of which belong to the same tetragonal crystal system deduced from the  $TiSi_2$  structure.

Nano-structuring via chemical or physical processes has been well known to be able to improve the TE properties of semiconductors.

Instead of complex chemical controlling to achieve nanowires or nano-particles<sup>[15,16]</sup>, a simple and cost-effective approach of nano-structuring of melted  $(Bi_{1-x}Sb_x)_2Te_3$  bulk material combining ball milling and subsequent hot pressing was reported to have improved the  $ZT_{max}$  up to 40%<sup>[17]</sup>. Motivated by this concept, we have applied higher energy ball milling on melted polycrystalline HMS and studied the effect on the phase constitution, microstructure and TE performance of the subsequently hot-pressed samples.

## 2. Experimental

A HMS ingot ( $Mn_{15}Si_{26}$ ) was prepared by vacuum levitation melting from pure Mn (99.99%) and Si (99.999%). The as-melted ingot was ground to powders of about 300 meshes in size, which were then subjected to ball milling in a stainless steel vial with a speed of 300 rpm. The ball milling was carried out in hexane for  $10 \times 3^n$  minutes ( $n = 0, 1, 2, 3, 4, 5$ ) with a ball-to-powder weight ratio of 10:1. Collected powders after ball milling were charged into a graphite die of 12 mm in diameter, followed by hot pressing under 100 MPa at 1173 K for 1 h in argon. The investigated samples in this work are named with the following rule, for example, BM5 for powders ball-milled for  $10 \times 3^5$  min and HP5 for pellet hot-pressed from BM5.

The crystal structures were studied by XRD with a Siemens D5000 diffractometer using  $Cu K\alpha$  radiation ( $\lambda = 1.5406 \text{ \AA}$ ). The morphologies were observed using SEM. Compositional analysis was carried out by ICP (Perkin Elmer

Optical Emission Spectrometer Optima 5300 DV). Seebeck coefficients  $\alpha$  were measured in vacuum from room temperature (RT) to 973 K. The electrical conductivity  $\sigma$  measurement was performed by the standard four-probe DC method. The thermal diffusivity  $D$  and  $c_p$  was measured on a laser flash apparatus (Netzsch LFA 427 and Netzsch DSC-404). The thermal conductivity was then calculated by  $\kappa = Dc_p\rho$ , where  $\rho$  is the sample density measured with the Archimedes method,  $D$  the thermal diffusivity and  $c_p$  the specific heat.

### 3. Results and Discussions

Fig. 1 and Fig. 2 show the XRD patterns of the ball-milled powders and hot-pressed pellets of HMS, respectively. It is clear that the as-melted ingot (BM0) is composed of the dominating HMS phase (in this work identified as  $\text{Mn}_{15}\text{Si}_{26}$ , space group  $I\bar{4}2d$ ) and the minor phases MnSi (or  $\text{Mn}_{1-x}\text{Fe}_x\text{Si}$ ) and Si. The presence of MnSi and Si at the same time indicates the incomplete peritectic reaction between MnSi nucleus and the Si-rich melt as the melt is cooled down, owing to the slow diffusion of Si atoms into MnSi<sup>[18-19]</sup>. As the powders are ball-milled, the residual Si tends to disappear, while the MnSi (or  $\text{Mn}_{1-x}\text{Fe}_x\text{Si}$ ) phase remarkably increases with increasing ball-milling duration. In the sample BM5, the monosilicide has become the dominating phase compared with the non- or short-time ball-milled samples. We also observed an obvious decrease of the powder average grain size after ball milling from their broadened peaks. For the hot-pressed samples, the peaks are narrower than those of the powders, indicating grain growth during the hot pressing.

The SEM images of the ball-milled powders are shown in Fig. 3. We can see that the effect of ball milling on the change of grain size is remarkable. In sample BM1, the powder grain size was of micrometer scale, while in sample BM5 that was ball-milled for 43 hours the average grain size has decreased to 50–100 nm. Although we have achieved nano-structuring of the materials through ball milling, the TE properties were not expected to improve because of the simultaneously introduced MnSi (or  $\text{Mn}_{1-x}\text{Fe}_x\text{Si}$ ) phase that has metallic character. Anyway, we performed TE measurements on the samples to see how far the monosilicide affects the TE performance.

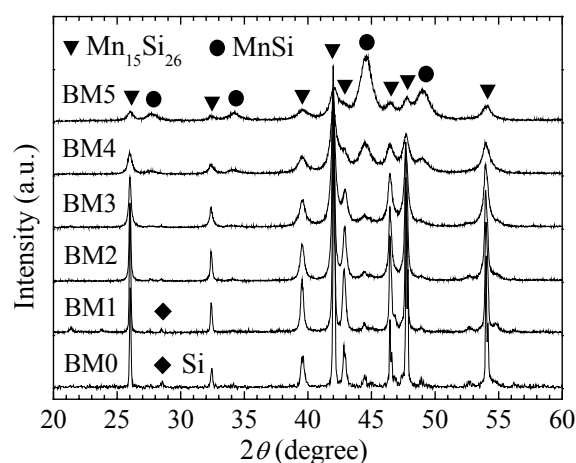


Fig. 1. XRD patterns of HMS powders with different ball milling duration.

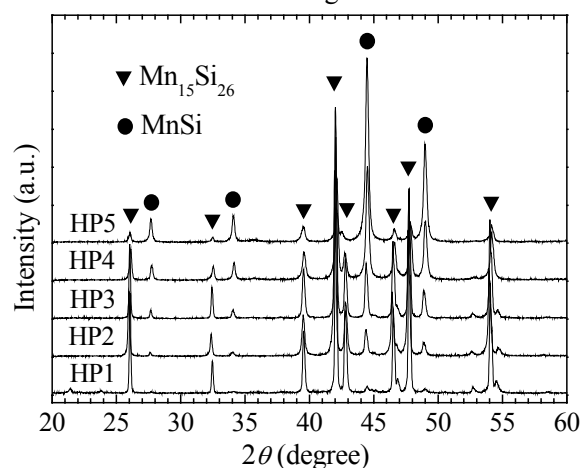


Fig. 2. XRD patterns of hot-pressed HMS pellets from ball-milled powders.

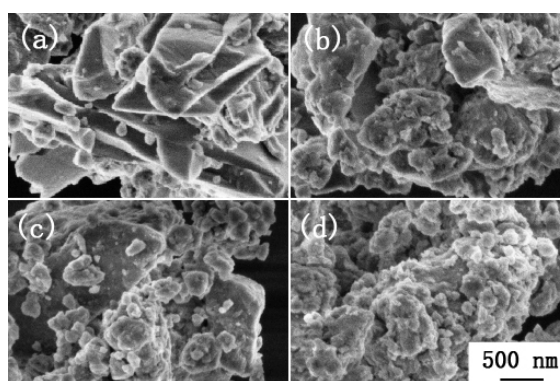


Fig. 3. SEM images of ball-milled powders. (a) BM1, (b) BM2, (c) BM3, (d) BM5

From Fig. 4 to Fig. 6 we can conclude that the Seebeck coefficient was dramatically reduced after ball milling, while the electrical and thermal conductivity were increased and thus the TE performance was deteriorated. An exception on the electrical conductivity happened for the sample HP2, exhibiting the lowest value. The reason is not yet clear. Further analyses need to be carried out to explain this. The  $ZT_{\text{max}}$  in the present work occurs in sample HP1 to be 0.3 at

520 °C, which is only half of the  $ZT_{\max}$  reported in the literature for polycrystalline HMS<sup>[20]</sup>, where a single phase of semiconducting  $\text{MnSi}_{1.75}$  was achieved synthesized by mechanical alloying with Si excess. On this view, the phase purity and stability should rate the most important factors for the TE performance of HMS.

Table. 1. Atomic ratios of elements in ball-milled powders from ICP results.

Sample	Fe/Mn (%)	Si/Mn	Si/(Mn+Fe)
BM0	–	1.704	1.704
BM1	5.035	1.593	1.517
BM2	8.664	1.572	1.447
BM3	4.127	1.479	1.421
BM4	12.05	1.457	1.301
BM5	25.82	1.395	1.109

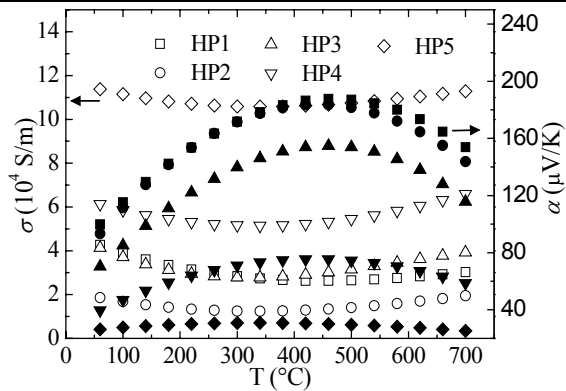
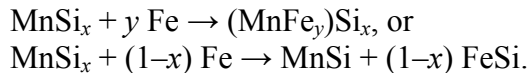


Fig. 4. Electrical conductivity  $\sigma$  and Seebeck coefficient  $\alpha$  of hot-pressed samples.

The phase transformation from HMS to  $\text{MnSi}$  (or  $\text{Mn}_{1-x}\text{Fe}_x\text{Si}$ ) presented in this work was not expected and few related reports were found. This phenomenon should be explained before trying to improve its TE performance via nanostructuring by ball milling. To get more clues about this, compositional analyses of powders were carried out. From table 1 it is clear to see that an overall Si loss and an iron introduction (up to 25 % in sample BM5) have happened during ball milling.

The high iron content is due to the contamination from stainless steel vials and balls and could be introduced through the following reaction:



From EDX measurements we observed that iron was incorporated both into  $\text{MnSi}$  and HMS phases. However it is difficult to define from the present XRD results, although minor peak shifts were observed, whether the iron was alloyed with the  $\text{MnSi}$  phase or forms a third phase  $\text{FeSi}$ .

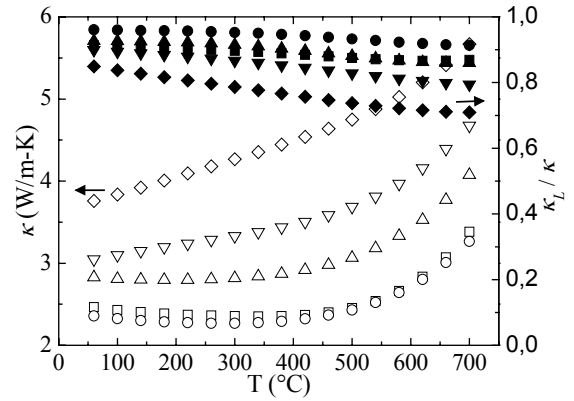


Fig. 5. Thermal conductivity  $\kappa$  and the lattice contribution  $\kappa_L / \kappa$  of hot-pressed samples.

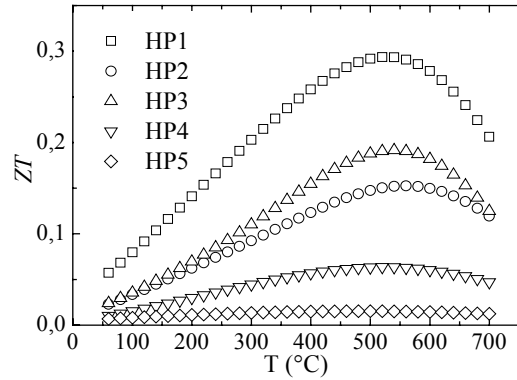


Fig. 6. Dimensionless figure of merit  $ZT$  of hot-pressed samples

The  $\text{MnSi}$  and  $\text{FeSi}$  phases belong to the same structure and their peak positions are very close to each other. According to literature<sup>[3]</sup> the solubility of Fe in the HMS matrix reaches up to 30% ( $\text{Mn}_{0.7}\text{Fe}_{0.3}\text{Si}_{1.682}$ ). So we can conclude that the status of iron is much more probable alloyed to either  $\text{MnSi}$  or HMS rather than as a third phase  $\text{FeSi}$ .

The ex-situ Fe introduction was firstly supposed to be the reason for the appearance of metallic phase. However, noting that the Si/Mn atomic ratio was monotonically decreased, one can infer that the iron introduction is not the only reason for the overall Si-loss. In order to find some relationships we tried changing the ball milling parameters, such as lowering the ball milling energy by decreasing the speed of rotation, or replacing the stainless steel balls and vials with agate ones to exclude the iron contamination. However, in both cases the  $\text{MnSi}$  (or  $\text{Mn}_{1-x}\text{Fe}_x\text{Si}$ ) phase was easily evidenced by XRD. Meanwhile, it was also found that the amount of monosilicide increased monotonically as the ball milling energy was increased.

The overall Si loss in HMS during ball milling has till now no exact explanation given incomplete analysis results. The Si loss during

ball milling was also reported in the work of Umemoto<sup>[20]</sup>. It is difficult to confirm whether the Si loss or the ball milling itself causes the phase transformation. Taking a close view into the crystal structures of HMS<sup>[21]</sup>, one can see that the HMS single cells have unusually long  $c$  axes that vary with different phases while the  $a$  axis for all phases are the same. The  $c/a$  ratio of HMS, for example in  $Mn_{27}Si_{47}$  and  $Mn_{15}Si_{26}$  reaches 21.3 and 11.8, respectively, which is extraordinarily large compared with the cubic MnSi phase with  $c/a$  equals 1. From the viewpoint of crystal internal energy, it is reasonable to assume that the chimney-laddered HMS structures could be unstable under high mechanical impact. If the external energy introduced by ball milling was high enough to overcome the internal combining energy barrier in the HMS structures, the long  $c$  axis structures could possibly be broken into smaller ones having a shortened  $c$  axis. This kind of structural destruction coupled with the self-coordination in lattice parameters and composition could then result in more and more MnSi as the duration or the energy of ball milling was increased. However, for confirmation of this assumption, other detailed analyses and computational simulation are still needed.

#### 4. Conclusion

We presented the effect of ball milling on the phase constitution, microstructure and the TE properties of the as-melted HMS. Iron contamination through ball-milling was observed. Instead of obtaining HMS single phases with nano-scaled particles, we firstly observed a remarkable phase transformation and overall Si loss after the ball milling. The amount of the metallic MnSi phase (or  $Mn_{1-x}Fe_xSi$ ), which deteriorates the TE performance of the material, increases with increasing ball milling duration and energy. This phase transformation is hypothetically attributed to the instability of the long  $c$  axis structures of HMS phases under high energy mechanical treatment. Further investigations are suggested for the explanation of this phenomenon.

#### Acknowledgements

The authors would like to thank W. Schönau from Institute of Materials Research, German Aerospace Center (DLR) for thermal conductivity measurement. This work was supported by the Sandwich Program of German Academic Exchange Service (DAAD), the National Basic Research Program of China (Grant

No. 2007CB607502) and the National Science Foundation of China (Grant No. 50522203).

#### References

1. J.E. Mahan, *Thin Solid Films* **461** (2004) 152-159.
2. V.E. Borisenko, ed., *Semiconducting Silicides*. Springer, 2000, Berlin.
3. M.I. Fedorov and V.K. Zaitsev, in *Thermoelectrics Handbook*, D.M. Rowe, ed., p.31. CRC Press, 2005, New York.
4. M.I. Fedorov, V.K. Zaitsev, F.Y. Solomkin, and M.V. Vedernikov, *Tech. Phys. Lett.* **23** (1997) 602-603.
5. I. Kawasumi, M. Sakata, I. Nishida, and K. Masumoto, *J. Mater. Sci.* **16** (1981) 355-366.
6. I. Kawasumi, M. Sakata, I. Nishida, and K. Masumoto, *J. Cryst. Growth* **49** (1980) 651-658.
7. T. Kojima, I. Nishida, and M. Sakata, *J. Cryst. Growth* **47** (1979) 589-592.
8. Q.R. Hou, W. Zhao, Y.B. Chen, D. Liang, X. Feng, H.Y. Zhang, and Y.J. He, *Appl. Phys. A* **86** (2007) 385-389.
9. Q.R. Hou, W. Zhao, Y.B. Chen, D. Liang, X. Feng, H.Y. Zhang, and Y.J. He, *phys. stat. sol. (a)* **204** (2007) 3429-3437.
10. Q.R. Hou, W. Zhao, H.Y. Zhang, Y.B. Chen, and Y.J. He, *phys. stat. sol. (a)* **203** (2006) 2468-2477.
11. O.G. Karpinskii and B.A. Evseev, *Neorg. Mater.* **5** (1969) 525.
12. O. Shwomma, A. Preisinger, H. Nowotny, and A. Wittman, *Monatsh. Chem.* **95** (1964) 1527.
13. H.W. Knott, M.H. Mueller, and L. Heaton, *Acta Crystallogr.* **23** (1967) 549-555.
14. G. Zwilling and H. Nowotny, *Monatsh. Chem.* **102** (1971) 672.
15. Y. Q. Cao, X. B. Zhao, T. J. Zhu, X. B. Zhang, and J.P. Tu, *Appl. Phys. Lett.* **92** (2008) 143106.
16. X. B. Zhao, X.H. Ji, Y.H. Zhang, T.J. Zhu, J.P. Tu, and X.B. Zhang, *Appl. Phys. Lett.* **86** (2005) 062111.
17. B. Poudel, Q. Hao, Y. Ma, A.M. Yucheng Lan, B. Yu, X. Yan, D.Z. Wang, A. Muto, D. Vashaee, X.Y. Chen, J.M. Liu, M.S. Dresselhaus, G. Chen, and Z.F. Ren, *Science* **320** (2008) **634-638**.
18. I. Nishida, K. Masumoto, I. Kawasumi, and M. Sakata, *J. Alloy. Compd.* **71** (1980) 293-301.
19. I. Aoyama, M.I. Fedorov, V.K. Zaitsev, F.Y. Solomkin, I.S. Eremin, A.Y. Samunin, M. Mukoujima, S. Sano, and T. Tsuji, *Jpn. J. Appl. Phys.* **44** (2005) 8562-8570.
20. M. Umemoto, Z.G. Liu, R. Omatsuzawa, and K. Tsuchiya, *Mate. Sci. Forum* **342-346** (2000) 918-923.
21. D.B. Migas, V.L. Shaposhnikov, A.B. Filonov, and V.E. Borisenko, *Phys. Rev. B* **77** (2008) 075205.